# Synchronized patterns induced by distributed time delays

Jie Zhou and Zonghua Liu
*Institute of Theoretical Physics and Department of Physics, East China Normal University, Shanghai, 200062, China*
(Received 28 January 2008; published 23 May 2008)

Considering the fact that the distances between coupled oscillators may delay the receiving of signals, we study here the influence of uniformly distributed delays in an array of coupled pendulums instead of studying the influence of the coupling strength. We find that with an increase of the range of distributed delays, the chaotic behaviors of the coupled arrays may be controlled and different synchronized patterns can be induced. An analytic solution is given to confirm the numerical results. This finding may provide further insight into information processing in neurons.

DOI: 10.1103/PhysRevE.77.056213 PACS number(s): 05.45.Gg, 05.45.Xt, 74.81.Fa

## I. INTRODUCTION

The controlling chaos and synchronization has been well studied during the last two decades [1,2], and a variety of approaches have been presented to implement this task, ranging from dissipative systems [3–9] to conservative systems [10]. Most are focused on the influence of the coupling strength. It is found that chaos can be controlled and the trajectories of chaotic systems can be stabilized to some specific unstable periodic orbits. Among these researches, one of the interesting findings is that, contrary to the function of disorder as destroying spatial and temporal regularity, disorder can be also used to control chaos in an array of Josephson junctions [11–13]. For example, the chaotic dynamics of an array of pendulums can be controlled by a small amount of disorder to the length or by some impurities.

Recently, this problem has been restudied and it is found that instead of controlling chaos by increasing the coupling strength, the chaotic dynamics of an array of pendulums can be even controlled only by randomizing the initial phases of the external forces at the individual oscillators [14,15]. The array remains chaotic if all the initial phases are taken as the same constant. However, when the initial phases are uniformly distributed in the interval $[-k\pi,+k\pi]$, the oscillations of the array will become regular for sufficiently large $k$. The mechanism is revealed by an effective random equation of motion governing the dynamics of the soliton center of mass [15].

Considering the fact that in most realistic physical and biological systems the interaction signal is transported through media such as sound, etc., we observe that the signal will take some time to pass through a finite distance, because of limited speed, to arrive at its destination and thus induce a time-delay in receiving the signal [16,17]. For example, in biological neural networks, the transmission delay is a sum of axonal, synaptic, and dendritic delays. Actually, the axon conduction velocities are proportional to its size and there is a distribution of axon diameters in the nervous system [18]. Moreover, it is reported that axons can generate time delays as large as 300 ms [19,20]. It has been also shown that neural connections are full of variable loops, such that the propagation time through loops can result in a large time delay [21]. This feature of delay has been widely studied in coupled oscillators, neurons [22,23], food webs, etc., and various phenomena have been uncovered, such as wave formation [24], amplitude death [25], synchronization [26–30], ecological stability [31–33], etc.

In this paper, we study an array of coupled pendulums with randomly distributed distances between any two neighbors and consider the effect of different distances as distributed time delays in the coupling interactions. Our principal results are as follows: (a) The distributed time delays or "disorder" can also stabilize the chaotic dynamics of the coupled system and thus have the same function with the distributed random phases [14,15]. (b) Different periodic patterns may show up with an increase of the range of distributed delays. (c) An analytic solution is given to confirm the numerical results.

The paper is organized as follows. In Sec. II, we present our model and show its numerical simulations. Then, in Sec. III, we give the model's analytic solution. Finally, discussions and conclusions are given in Sec. IV.

## II. DISTRIBUTED TIME-DELAY MODEL

We here consider a coupled chain of forced, damped, nonlinear pendulums, which is sometimes called a driven Frenkel-Kontorova chain or Josephson-junction chain. The coupling is considered to be diffusive and only allowed between neighbors. We introduce an independent time delay to each coupling line, which is taken from a uniformly distributed random number. The equations can be described as

$$\begin{aligned} ml^2\ddot{\theta}_n + \gamma\dot{\theta}_n = &- mgl\,\sin\,\theta_n + \tau' + \tau\sin(\omega t + \varphi_n) \\ &+ s[\theta_{n+1}(t-\tau_{n+1}) + \theta_{n-1}(t-\tau_{n-1}) \\ &- 2\theta_n(t-\tau_n)], \\ n = 1,2,\ldots,N, \end{aligned} \tag{1}$$

where the parameters are taken as follows: the mass of the oscillator is $m=1$, the length $l=1$, the acceleration due to gravity $g=1$, the damping $\gamma=0.75$, the dc torque $\tau'=0.7155$, the ac torque $\tau=0.4$, the angular frequency $\omega=0.25$, the coupling strength $s=0.5$, and the initial phase $\varphi_n=0$. The time delay $\tau_n$ is a uniformly distributed random number in $[0,kh]$ with $h=0.001$ and $kh$ denoting the range of distributed delays. And periodic boundary conditions are

 

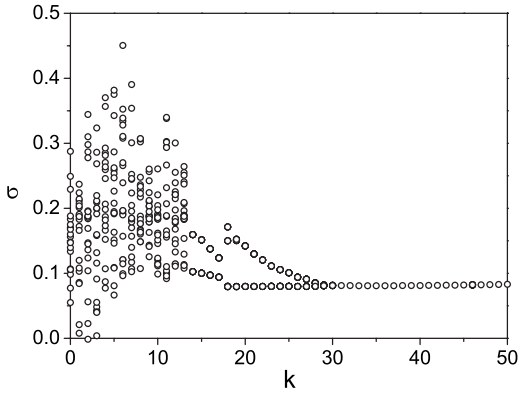


FIG. 1. How the average velocity $\sigma$ depends on the distribution parameter $k$ for $N=50$, where $\sigma$ is taken at $t=60T,61T,\ldots,80T$ for each $k$.

used—i.e., $\theta_0=\theta_N$ and $\theta_{N+1}=\theta_1$. In the following numerical simulations, we fix $N=50$ unless specified otherwise.

For understanding how the range $kh$ of distributed delays influences the global spatiotemporal behavior of Eq. (1), we consider the average velocity

$$\sigma(jT)=\frac{1}{N}\sum_{n=1}^{N}\dot{\theta}_n(jT) \tag{2}$$

at times that are integer multiples of the forcing period $T=2\pi/\omega$. We find that the oscillations become periodic patterns in the form of $1T,2T,3T,\ldots$ attractors for sufficiently large $k$. Figure 1 shows how $\sigma$ changes with $k$ for $N=50$, where $\sigma$ is measured at $t=60T,61T,\ldots,80T$ for each $k$. It is easy to see that the system becomes $2T$ attractors when $k$ is larger than 13 and a $1T$ attractor when $k$ is larger than 30.

How do the collective behaviors in Fig. 1 show up? For understanding its mechanism, we investigate the evolution of each individual oscillator and find that an increase of the range of distributed delays will make its behavior stabilize gradually. With an increase of $k$, the stabilized behavior will change from chaotic to periodic. When $k$ is over some critical value, the competition of the distributed asymmetric couplings causes all oscillators to stay in a stationary state—i.e., periodic patterns. Figure 2 shows four typical evolutions of $k=0$, 15, 25, and 40, respectively. Obviously, Fig. 2(a) is a chaotic attractor, Figs. 2(b) and 2(c) are two different $2T$ attractors with alternative long and short segments, and Fig. 2(d) is a $1T$ attractor. Their averages give just the values observed in Fig. 1.

The difference between the patterns of $2T$ attractors can be seen more clearly in Fig. 3 where the velocities are unfolded by the node positions. Figures 3(a) and 3(b) represent the two distinct distributions of velocity on the Poincaré section $t=jT$ for $k=15$ and Figs. 3(c) and 3(d) the distributions of velocity for $k=25$. It is easy to see that there is a soliton-like wave in the array and the shapes of the solitons are different for the cases $k=15$ and 25, indicating that they belong to different $2T$ attractors.

Figures 1 and 2 are for a fixed set of time delays. For a given $k$, there are numerous sets of time delays satisfying the uniform distribution. If the stabilized pattern or attractor depends on the chosen set of time delays, we may observe a variety of patterns for the same $k$. However, our numerical simulations show that the patterns are somehow robust to the sets of time delays and the degree of robust depends on $k$. For example, we may observe a few kinds of patterns for a medium $k$ and only one pattern for large $k$. For illustrating the weights of different patterns at a given $k$, we calculate the possibility for the system to reach a $1T,2T,4T$ and chaotic attractors after $t=60T$. Figure 4 shows how the possibility $P$ changes with the disorder parameter $k$. It is easy to see that the dynamics of the oscillators is mainly remained chaotic when $k$ is less than 13, but dominated by $1T$ pattern when $k$ is over 30. In between these two regimes, it is possible for other periodic patterns to show up.

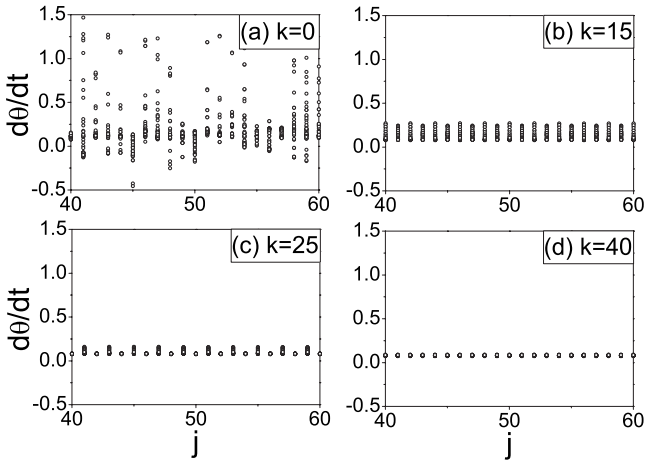


FIG. 2. Typical evolutions of individual oscillators for $N=50$ where (a), (b), (c), and (d) represent the cases of $k=0$, 15, 25, and 40, respectively.

With an increase of $k$, except for observing the transition from chaotic to periodic attractors, we also observe that the variation range of velocities becomes narrower and narrower; i.e., the oscillators become largely synchronous. For measuring how the disorder parameter $k$ influences the syn-

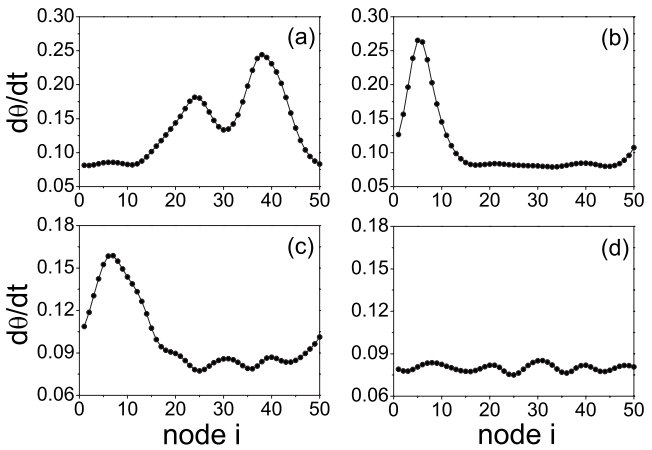


FIG. 3. The shapes of $2T$ attractors on the Poincaré section $t=jT$ where (a) and (b) denote the case of $k=15$ and (c) and (d) the case of $k=25$.

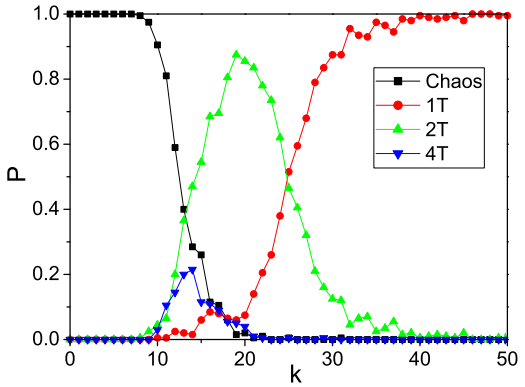


FIG. 4. (Color online) Probability $P$ of chaotic dynamics and several regular behaviors versus the disorder parameter $k$ in a chain of $N=50$ coupled oscillators. $P$ is determined by averaging over 200 different sets of time delays.

chronization, we introduce the self-correlation and the cross correlation. The self-correlation is defined as follows:

$$D = \frac{1}{N}\sum_i D_i, \tag{3}$$

with

$$D_i = \frac{\int_{T_0}^{T_0+T} dt\ \dot{\theta}_i(t)\dot{\theta}_i(t+T)}{\left[\int_{T_0}^{T_0+T} dt\ \dot{\theta}_i^2(t)\int_{T_0}^{T_0+T} dt\ \dot{\theta}_i^2(t+T)\right]^{1/2}}, \tag{4}$$

where $T_0$ is a time after the transient process. The "solid circles" in Fig. 5 show how $D$ changes with $k$ where the average is performed over 200 different sets of the time delays and the error bars show the standard deviation. It is easy to see that $D$ is not very sensitive to $k$ when $k<10$, implying

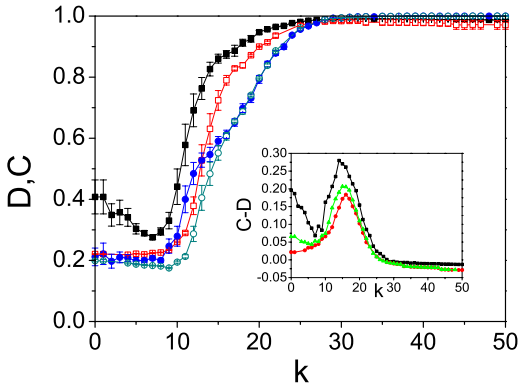


FIG. 5. (Color online) Correlations $D$ and $C$ versus $k$, where the solid circles and solid squares represent the self-correlation and cross correlation for $N=50$, respectively, and the open ones denote the corresponding case of $N=200$, respectively. The inset shows the distance between $C$ and $D$ with squares, triangles, and circles denoting the cases of $N=50$, 100, and 200, respectively. The average is performed over 200 different sets of time delays, and the error bars show the standard deviation.

that the small range of the distribution of delays does not have much influence on $D$. After that, $D$ becomes sensitive to $k$ and increases monotonously with $k$ until $k=30$, indicating the appearance of periodic patterns and that the patterns are gradually transformed into low-periodic patterns, such as a $1T$ attractor. Further increase of $k$ (for $k>30$) causes $D$ to reach unity and then remain there, indicating that the pattern becomes strictly a $1T$ attractor.

Except for self-correlation, we are also interested in the mutual synchronization among different oscillators. For measuring this relationship, the cross correlation is defined as

$$C = \frac{2}{N(N-1)}\sum_{i<j} C_{ij}, \tag{5}$$

with

$$C_{ij} = \frac{\int_{T_0}^{T_0+T} dt\ \dot{\theta}_i(t)\dot{\theta}_j(t)}{\left[\int_{T_0}^{T_0+T} dt\ \dot{\theta}_i^2(t)\int_{T_0}^{T_0+T} dt\ \dot{\theta}_j^2(t)\right]^{1/2}}, \tag{6}$$

where $C_{ij}$ denotes the correlation between the $i$th and $j$th oscillators. The solid squares in Fig. 5 show how $C$ changes with $k$. Comparing the solid circles with the solid squares in Fig. 5 we see that curves $D$ and $C$ are very similar; i.e., both increase monotonously for $10<k<30$ and then remain at unity for $k>30$. As the cross correlation measures the correlation among the oscillators, the unity of $C$ for $k>30$ means that a significant $k$ makes an approximate synchronization possible although the coupling terms on each individual oscillator are asymmetric.

It is interesting to study how the self-correlation and cross correlation depend on the number of oscillators. By increasing $N$, we find that the phase transition becomes more clear; see the open circles and open squares in Fig. 5 for $D$ and $C$ with $N=200$, respectively. However, when $N$ increases further, such as $N>500$, we observe that for larger $k$, the self-correlation $D$ will stay around unity, but the cross correlation $C$ will decrease. The distance of $C$ away from unity for $k>25$ will increase with $N$. Thus, we infer that in the thermodynamic limit, the transition to unity will be kept for the $D$ curve, but disappear for the $C$ curve. We will explain it later. On the other hand, we notice that the difference between $C$ and $D$ shows a resonance for the not very large $N$; see the inset in Fig. 5 for $N=50$, 100, and 200, respectively. The reason can be understood from Fig. 4 where there are multiple attractors for $10\leq k\leq 30$. As $D$ measures the self-correlation, it does not depend on concrete periodic patterns or chaos. However, $D$ will be influenced by these multiple attractors. For example, when the oscillator $i$ is in period 1 and the oscillator $j$ is in period 4, their different periods will make it difficult for $C$ to be close to unity, resulting in a difference $C-D$. This is what we observe in the inset of Fig. 5.

## III. ANALYTIC SOLUTION

For understanding the mechanism of stabilizing chaos by uniformly distributed time delays, we now do some theoret-

ical analysis on Eq. (1). Following the analytic approach used in Refs. [26,34], we will formulate the general master stability functions for the uniformly distributed time delays. The equation is as follows:

$$\dot{\mathbf{x}}_i = \mathbf{F}(\mathbf{x}_i) + s\sum_j G_{ij}\mathbf{H}[\mathbf{x}_j(t-\tau_{ij})], \tag{7}$$

where $\mathbf{x}_i$ is the three-dimensional dynamical variable vector of Eq. (1) for node $i$ with $x(1)=\theta$, $x(2)=\dot{\theta}$, and $x(3)=\omega t$. The uncoupled dynamics for each node is $\dot{\mathbf{x}}_i=\mathbf{F}(\mathbf{x}_i)$. $\mathbf{H}$: $R^m \to R^m$ is the coupling function, $\mathbf{G}$ is an $N\times N$ matrix which determines node-to-node coupling, and they can be expressed as

$$\mathbf{G} = \begin{pmatrix} -2 & 1 & 0 & \cdots & 1 \\ 1 & -2 & 1 & \cdots & 0 \\ 0 & 1 & -2 & \cdots & 0 \\ \vdots & \vdots & \vdots & \vdots & \vdots \\ 1 & 0 & \cdots & 1 & -2 \end{pmatrix}$$

and

$$\mathbf{H} = \begin{pmatrix} 0 & 0 & 0 \\ 1 & 0 & 0 \\ 0 & 0 & 0 \end{pmatrix}.$$

The symmetric matrix $G$ has eigenvalues $0=\lambda_1>\lambda_2\geq\lambda_3\geq\cdots\geq\lambda_N$.

Comparing with the characteristic time of the system—i.e., the period $2\pi/\omega$—$\tau_{ij}$ ($\tau_{ij}\leq kh$) is a small quantity, and thus Eq. (7) can be approximately written as

$$\dot{\mathbf{x}}_i \approx \mathbf{F}(\mathbf{x}_i) + s\sum_j G_{ij}\mathbf{H}[\mathbf{x}_j(t) - \tau_{ij}\dot{\mathbf{x}}_j(t)]. \tag{8}$$

For a synchronization manifold $\mathbf{x}_1=\mathbf{x}_2=\cdots=\mathbf{x}_N$, the average of Eq. (8) will be invariant. Taking the averages as $\langle\cdots\rangle=\frac{1}{\tau'}\int_0^{\tau'}(\cdots)d\tau_{ij}$ with $\tau'=kh$, we get an effective deterministic equation

$$\dot{\mathbf{x}}_i = \mathbf{F}(\mathbf{x}_i) + s\sum_j G_{ij}\mathbf{H}[\mathbf{x}_j(t) - \tau\dot{\mathbf{x}}_j(t)], \tag{9}$$

where $\tau=\tau'/2$ and brackets are omitted for short. Letting $\mathbf{x}$ be the synchronization manifold and $\xi_i$ be the variational vector; then, the variational equation of the $i$th oscillator is

$$\dot{\xi}_i = D\mathbf{F}(\mathbf{x})\xi_i + s\sum_j G_{ij}D\mathbf{H}(\xi_j - \tau\dot{\xi}_j). \tag{10}$$

To assess the linear stability of the synchronous state $\mathbf{x}$, we diagonalize the variational equation (10) and check that the perturbations transverse to the synchronized manifold are damped. Diagonalizing the matrix $G$ by $SGS^{-1}$ and letting $\xi=[\xi_1,\ldots,\xi_N]^T$ and $\eta\equiv[\eta_1,\ldots,\eta_N]^T=S\xi$, we obtain

$$\begin{aligned}\dot{\eta}_j &= [\mathbf{I} + s\tau\lambda_j D\mathbf{H}]^{-1}[D\mathbf{F} + s\lambda_j D\mathbf{H}]\eta_j \\ &= [D\mathbf{F} + s\lambda_j D\mathbf{H} - s\tau\lambda_j D\mathbf{H}D\mathbf{F}]\eta_j,\end{aligned} \tag{11}$$

where the condition $\mathbf{H}^2=0$ is applied. Equation (11) is the master stability equation.

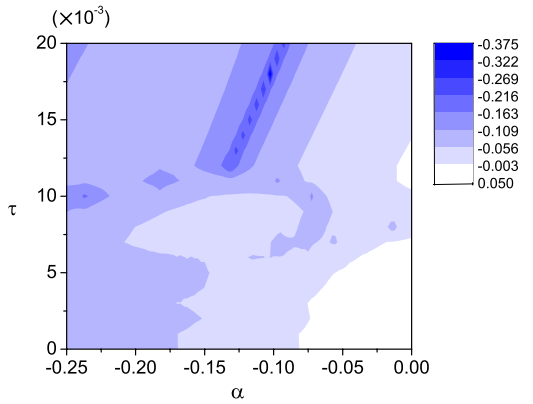


FIG. 6. (Color online) Master stability function in the $(\alpha,\tau)$ parameter plane which is performed by 200 different samplings.

The diffusive coupling matrix $G$ in a circular array gives eigenvalues of $\lambda_j=-4\sin^2(\pi j/N)$, with $j=0,\ldots,N-1$. For $j=0$, we have the variational equation for the synchronization manifold ($\lambda_0=0$). All other $j$'s correspond to transverse eigenvectors or transverse modes. For a specific coupling strength $s$, if the $j-1$ variational equations with $j=1,\ldots,N-1$ have negative Lyapunov exponents, the system will be synchronized. Moreover, if all the Lyapunov exponents of these equations, including the case of $j=0$, are nonpositive, the system will be both periodic and synchronized. We calculate the maximum transverse Lypunov exponent (MTLE) for the generic variational equation

$$\dot{\eta} = [D\mathbf{F} + \alpha D\mathbf{H} - \tau\alpha D\mathbf{H}D\mathbf{F}]\eta \tag{12}$$

as a function of $\alpha$ and $\tau$ with $\alpha=s\lambda_1$. Figure 6 shows the master stability function: the MTLE in $(\alpha,\tau)$ parameter space, which is obtained by performing 200 different samplings of the initial value of Eq. (12). From Fig. 6 we see that for sufficiently larger $\tau(k)$—say, $\tau>13\times10^{-3}$ or $k>13$—all the MTLEs will be negative, which is approximately consistent with the numerical simulations in Figs. 1 and 4.

The synchronization of coupled oscillators is determined by the MTLE of the transverse mode, $\lambda_1$. The system will be synchronized when $\lambda_1$ is negative and nonsynchronized when $\lambda_1$ is non-negative. And the stabilization of chaotic behavior is determined by the largest Lyapunov exponent of the system, $\lambda_0$. The system is chaotic when $\lambda_0>0$ and nonchaotic when $\lambda_0<0$. When $N\to\infty$—i.e., the thermodynamic limit—we have $\lambda_1\to\lambda_0\to0$. Therefore, MTLE becomes non-negative and causes the synchronization among oscillators to become difficult. This is the reason why we observe numerically that the transition to unity in $C$ disappears for large $N$.

Figure 6 also shows how the coupling strength $s$ influences the synchronization. As $\alpha=s\lambda_1$, larger $s$ means larger $\alpha$. Hence the horizontal axis of Fig. 6 denotes the coupling strength and its vertical axis denotes the time delay. It is easy to see that when $\tau=0$—i.e., when there is no time delay—the MTLE will become negative only when the coupling strength is large enough or $|s\lambda_1|>0.08$. However, when $\tau$ is large enough—i.e., $\tau>13h$—the MTLE becomes negative even when the coupling strength is very small; see the verti-

cal axis of $\alpha=0$. Therefore, we may think that the induced synchronization is a new phenomenon when $s$ is very small. In general, for finite $s$, Fig. 6 shows that the time-delay $\tau$ is in favor of synchronization.

## IV. DISCUSSIONS AND CONCLUSIONS

In the communication of real physical or biological systems, time delays in signals are unavoidable because of different distances or different speeds of signal transportation. Especially, in the communication of neurons, the time delays are most likely different because the distance between different neurons differs. Our results suggest that the signal transmission can be seriously influenced by the distributed time delays and significant delays may result in synchronization and therefore benefit the signal transmission. This finding may provide further insight into information processing in biological systems.

In conclusion, we have uncovered a phenomenon of controlling chaotic dynamics with distributed time delays. This approach is equivalent to the approach of distributed random phases. When the parameter $k$ is significant, the distributed time delays can cause the system to become periodic patterns. The oscillators can even become approximately synchronized when $k$ is large enough.

## ACKNOWLEDGMENTS

This work was supported by the NNSF of China under Grants No. 10775052 and No. 10635040, by SPS under Grant No. 05SG27, by NCET-05-0424, by Program for Changjiang Scholars and Innovative Research Team, and by PhD Program Scholarship Fund of ECNU 2007.

[1] A. Pikovsky, M. Rosenblum, and J. Kurths, *Synchronization: A Universal Concept in Nonlinear Sciences* (Cambridge University Press, Cambridge, England, 2001).
[2] S. Boccaletti, J. Kurths, G. Osipov, D. L. Valladares, and C. Zhou, Phys. Rep. **366**, 1 (2002).
[3] E. Ott, C. Grebogi, and J. A. Yorke, Phys. Rev. Lett. **64**, 1196 (1990).
[4] L. M. Pecora and T. L. Carroll, Phys. Rev. Lett. **64**, 821 (1990).
[5] M. G. Rosenblum, A. S. Pikovsky, and J. Kurths, Phys. Rev. Lett. **76**, 1804 (1996); **78**, 4193 (1997).
[6] N. F. Rulkov, M. M. Sushchik, L. S. Tsimring, and H. D. I. Abarbanel, Phys. Rev. E **51**, 980 (1995).
[7] K. Pyragas, Phys. Rev. E **56**, 5183 (1997); **54**, R4508 (1996).
[8] Z. Zheng and G. Hu, Phys. Rev. E **62**, 7882 (2000).
[9] Zonghua Liu and Shigang Chen, Phys. Rev. E **56**, 7297 (1997); **55**, 6651 (1997); Z. Liu, Y.-C. Lai, and M. A. Matias, *ibid.* **67**, 045203(R) (2003).
[10] Zonghua Liu and Shigang Chen, Phys. Rev. E **56**, 168 (1997); **56**, 1585 (1997); Chin. Phys. Lett. **14**, 816 (1997).
[11] Y. Braiman, W. L. Ditto, K. Wiesenfeld, and M. L. Spano, Phys. Lett. A **206**, 54 (1995); Y. Braiman, J. F. Linder, and W. L. Ditto, Nature (London) **378**, 465 (1995).
[12] A. Gavrielides, T. Kottos, V. Kovanis, and G. P. Tsironis, Phys. Rev. E **58**, 5529 (1998); Europhys. Lett. **44**, 559 (1998).
[13] B. Hu, Z. Liu, and Z. Zheng, Commun. Theor. Phys. **35**, 425 (2001); B. Hu and Z. Liu, Int. J. Bifurcation Chaos Appl. Sci. Eng. **11**, 1461 (2001).
[14] S. F. Brandt, B. K. Dellen, and R. Wessel, Phys. Rev. Lett. **96**, 034104 (2006).
[15] R. Chacon and P. J. Martinez, Phys. Rev. Lett. **98**, 224102 (2007).
[16] T. Omi and S. Shinomoto, Phys. Rev. E **76**, 051908 (2007).
[17] P. Gong and C. vanLeeuwen, Phys. Rev. Lett. **98**, 048104 (2007).
[18] R. Miller, in *Oscillatory Event-related Brain Dynamics*, edited by C. Pantev *et al.* (Plenum, New York, 1994), pp. 53–57.
[19] H. A. Swadlow, J. Neurophysiol. **54**, 1346 (1985).
[20] F. Aboitiz *et al.*, Brain Res. **598**, 143 (1992).
[21] M. Reigl, U. Alon, and D. B. Chklovskii, BMC Biol. **2**, 25 (2004).
[22] P. C. Bressloff, J. Phys. A **27**, 4097 (1994); Phys. Rev. Lett. **82**, 2979 (1999).
[23] M. P. James, S. Coombes, and P. C. Bressloff, Phys. Rev. E **67**, 051905 (2003).
[24] T. W. Ko, S. O. Jeong, and H. T. Moon, Phys. Rev. E **69**, 056106 (2004).
[25] A. Prasad, Phys. Rev. E **72**, 056204 (2005).
[26] M. Dhamala, V. K. Jirsa, and M. Ding, Phys. Rev. Lett. **92**, 074104 (2004).
[27] D. Huber and L. S. Tsimring, Phys. Rev. Lett. **91**, 260601 (2003).
[28] S. Kim, S. H. Park, and C. S. Ryu, Phys. Rev. Lett. **79**, 2911 (1997).
[29] F. M. Atay and O. Karabacak, SIAM J. Appl. Dyn. Syst. **5**, 508 (2006).
[30] Z. Liu and P. M. Hui, Physica A **383**, 714 (2007).
[31] N. MacDonald, *Time Lags in Biological Models,* Lecture Notes in Biomathematics, Vol. 27 (Springer-Verlag, Berlin, 1978).
[32] N. MacDonald, *Biological Delay Systems: Linear Stability Theory* (Cambridge University Press, Cambridge, England, 1989).
[33] C. W. Eurich, A. Thiel, and L. Fahse, Phys. Rev. Lett. **94**, 158104 (2005).
[34] L. M. Pecora and T. L. Carroll, Phys. Rev. Lett. **80**, 2109 (1998).